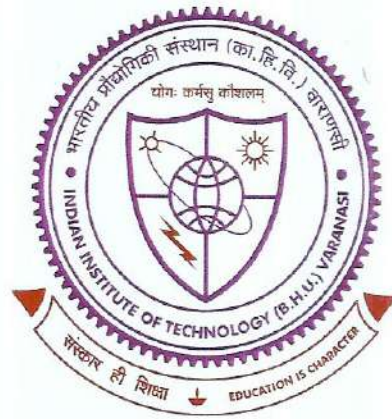


**Phase Evolution, Thermal Stability, Mechanical, Wear and
Biocompatibility Properties of High Entropy Steels
and Fe-based High Entropy Alloys**



**Thesis submitted in partial fulfillment for the
Award of Degree**

Doctor of Philosophy

By

Harsh Jain

**DEPARTMENT OF CERAMIC ENGINEERING
INDIAN INSTITUTE OF TECHNOLOGY
(BANARAS HINDU UNIVERSITY)
VARANASI- 221005
INDIA**

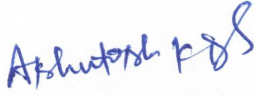
Roll No. 17031502

2023

CERTIFICATE

It is certified that the work contained in this thesis titled “Phase Evolution, Thermal Stability, Mechanical, Wear and Biocompatibility Properties of High Entropy Steels and Fe-based High Entropy Alloys” by “Harsh Jain” has been carried out under my supervision and that this work has not been submitted elsewhere for a degree.

It is further certified that the student has fulfilled all the requirements of Comprehensive, Candidacy and SOTA for the award of Ph.D. degree.



Dr. Ashutosh Kumar Dubey
(Supervisor)

Associate Professor and Head
Department of Ceramic Engineering
Indian Institute of Technology (B.H.U.), Varanasi
Varanasi-221005, Uttar Pradesh, India

Associate Professor
Department of Ceramic Engineering
सेरामिक अभियान्त्रिकी विभाग
Indian Institute of Technology (B.H.U.)
भारतीय प्रौद्योगिकी संस्थान (का०हि०वि०वि०)
Varanasi-221005/वाराणसी-221005



Prof. N K Mukhopadhyay
(Co-supervisor)

Professor in Physical Metallurgy
Department of Metallurgical Engineering
Indian Institute of Technology (B.H.U.), Varanasi
Varanasi-221005, Uttar Pradesh, India

प्रचार्य/Professor
धातुकीय अभियान्त्रिकी विभाग
Department of Metallurgical Engg.
भारतीय प्रौद्योगिकी संस्थान (काशी हिन्दू विश्वविद्यालय)
Indian Institute of Technology (Banaras Hindu University)
वाराणसी-221005/Varanasi-221005

DECLARATION BY THE CANDIDATE

I, Harsh Jain, certify that the work embodied in this thesis is my own bonafide work and carried out by me under the joint supervision of **Dr. Ashutosh Kumar Dubey and Prof. Nilay Krishna Mukhopadhyay** for a period from **December 2017** to **December 2023**, at the **“Department of Ceramic Engineering”**, Indian Institute of Technology (BHU), Varanasi. The matter embodied in this thesis has not been submitted for the award of any other degree/diploma. I declare that I have faithfully acknowledged and given credits to the research workers wherever their works have been cited in my work in this thesis. I further declare that I have not wilfully copied any other's work, paragraphs, text, data, results, etc., reported in journals, books, magazines, reports dissertations, thesis, etc., or available at websites and have not included them in this thesis and have not cited as my own work.

Date: 07/12/2023

Place: Varanasi


(HARSH JAIN)

CERTIFICATE BY THE SUPERVISOR

This is to certify that the above statement made by the student is correct to the best of my knowledge.



Dr. Ashutosh Kumar Dubey
(Supervisor)

Associate Professor and Head
Department of Ceramic Engineering
Indian Institute of Technology (B.H.U.), Varanasi
Varanasi-221005, Uttar Pradesh, India

Associate Professor
Department of Ceramic Engineering
सेरामिक अभियान्त्रिकी विभाग
Indian Institute of Technology (B.H.U.)
भारतीय प्रौद्योगिकी संस्थान (का०हि०वि०वि०)
Varanasi-221005/वाराणसी-221005



Prof. N K Mukhopadhyay
(Co-supervisor)

Professor in Physical Metallurgy
Department of Metallurgical Engineering
Indian Institute of Technology (B.H.U.), Varanasi
Varanasi-221005, Uttar Pradesh, India

प्राचार्य / Professor
धातुक्रीय अभियान्त्रिकी विभाग
Department of Metallurgical Engg.
भारतीय प्रौद्योगिकी संस्थान (काशी हिन्दू विश्वविद्यालय)
Indian Institute of Technology (Banaras Hindu University)
वाराणसी-221005/Varanasi-221005

Forwarded by:



Dr. Ashutosh Kumar Dubey
(Head of Department)

Department of Ceramic Engineering
Indian Institute of Technology
(Banaras Hindu University)

Varanasi-221005, India
विभागाध्यक्ष/HEAD
सेरामिक अभियान्त्रिकी विभाग
Department of Ceramic Engineering
भारतीय प्रौद्योगिकी संस्थान (का०हि०वि०वि०)
Indian Institute of Technology (B.H.U.)
Varanasi-221005/वाराणसी-221005

COPYRIGHT TRANSFER CERTIFICATE

Title of the Thesis: Phase Evolution, Thermal Stability, Mechanical, Wear and Biocompatibility Properties of High Entropy Steels and Fe-based High Entropy Alloys

Candidate's Name: Harsh Jain

Copyright Transfer

The undersigned hereby assigns to the Indian Institute of Technology (Banaras Hindu University), Varanasi all rights under copyright that may exist in and for the above thesis submitted for the award of the *Doctor of Philosophy*.

Date: 07/12/2023

Place: Varanasi


(HARSH JAIN)

Note: However, the author may reproduce or authorize others to reproduce material extracted verbatim from the thesis or derivative of the thesis for author's personal use provided that the source and the Institute's copyright notice are indicated.

ACKNOWLEDGEMENT

I am deeply indebted to my supervisors Dr. Ashutosh Kumar Dubey and Prof. Nilay Krishna Mukhopadhyay for their invaluable advice, continuous support and motivations during the course of study. This endeavor would not have been possible without the immense support of my supervisors, which I have faced during my research work. Words cannot express my gratitude towards Prof. Mukhopadhyay for being very patient during my PhD journey, and for inspire me towards research.

I would like to extend my sincere thanks to my other RPEC members: Prof. Pralay Maiti (SMST) and Dr. Pradip Kumar Roy, Prof. Devendra Kumar, Prof. Rashmi Bala Rastogi (Department of Chemistry) for their valuable comments and suggestions towards improving my work. I am also thankful to Dr. Ashutosh Kumar Dubey, Head of the Department of Ceramic Engineering, and former Heads, Prof. Devendra Kumar and Prof. Vinay Kumar Singh for needful help for conducting my research work.

I am also grateful to Prof. R. K. Mandal for extending experimental facilities of XRD and DSC, Dr. Rampada Manna for HR-XRD, ICDD database and high temperature furnace of ARCIS, Prof. N.C. Santhi Srinivas for the facilities of material testing lab, Dr. Joysurya Basu for SEM and TEM, Dr. Kausik Chattopadhyay for extending help for the wire-cut EDM machine and pin-on-disk wear tester, Dr. Vikas Jindal and Dr. Subhasis Sinha for facility of vacuum arc melting. Many thanks to all the faculty who taught me at various stages. I would like to acknowledge Prof. K. K. Singh (coordinator CIF, IIT BHU) and Prof. Rajiv Prakash (former coordinator CIF, IIT BHU) for the facilities of Central instrument facilities, IIT BHU, Dr. Dibyendu Chakravarty (Scientist F, ARCI,

Hyderabad) and Prof. K. G. Prashanth (TalTech, Estonia) for the spark plasma sintering facility, Prof. N. V. Chalapathi Rao for extending EPMA facility.

Thanks, should also go to Mr. Lalit Kumar Singh for his invaluable and timely help for SEM and TEM experimental, Mr. Girish Sahoo and Mr. Anirban and other staffs of the CIF, IIT BHU for extending timely help for the experimentations. The administrative staffs in the Department of Ceramic and Metallurgical Engineering are quite helpful and supportive: Mr. Shailendra Kumar, Mr. Raj Kumar Mishra, Mr. Ashish Tripathi, Mr. Mansaram, Mr. J. P. Patel, Mr. Arun Prakash, Mr. Kamala Prasad, Mr. Chotey Lal, Mr. Anjani, Mr. Arun Prakash, Mr. J. P. Minz, Mr. Kamlesh Mishra. I'd like to recognize to my seniors Manish Kumar Singh, Abhishek Sharma, Vikas Shivam, Vivek Kumar Pandey, Preeti Kumari, Neera Singh, Yagnesh Shadangi, Premprakash Seth and Deepak Khare, and fellow colleagues Ankit, Aman, Vaibhav, Shankar, Dileep, Sandeep, Sarika, Priya, Priyatosh, Dharmendra, Urvashi, Rajat, Kuntal, Ritik and Marshall for their help and moral support though out my PhD journey.

I could not have undertaken this journey without the support of my family, especially Aakanksha my wife, and Riyanshi daughter for their love, patience, and encouragement, which helped me to get through this long journey in the most positive way. I am also grateful to all my friends and the people whose names are not mentioned here for extending their cooperation in any means.

Finally, I consider myself to be extremely privileged to have the opportunity to study in Indian Institute of technology (IIT)- Varanasi founded by legend Mahamana Pandit Madan Mohan Malaviya. At last, I thank the Almighty God, for giving me strength, and wisdom for successfully completing my thesis.

CONTENTS

List of Figures.....	ix
List of Tables.....	xxiv
Abbreviations.....	xxvii
Symbols.....	xxix
Preface.....	xxx
Chapter 1: Introduction and Literature Review.....	1
1.1 Historical sketch of alloys development.....	1
1.2 Historical background of HEAs.....	3
1.3 Core-effect of High Entropy Alloys.....	5
1.3.1 High entropy effect.....	5
1.3.2 Sluggish diffusion effect.....	6
1.3.3 Severe lattice distortion.....	6
1.3.4 Cocktail effect.....	7
1.4 Phase selection by parametric approach and CALPHAD.....	8
1.4.1 Parametric approach.....	8
1.4.2 CALPHAD modeling.....	12
1.5 High Entropy Steels and Fe-based HEAs.....	13
1.5.1 Synthesis.....	13
1.5.2 Structures.....	17
1.5.3 Thermal stability.....	18
1.6 Properties.....	20
1.6.1 Mechanical properties.....	21

1.6.2	Wear properties.....	26
1.6.3	Functional properties.....	29
1.7	Strengthening mechanisms.....	30
1.8	Application of High Entropy Steels and Fe-based HEAs.....	34
1.9	Motivation.....	35
1.10	Objective of the thesis.....	36
 Chapter 2: Experimental Details.....		37
2.1	Alloy designations.....	37
2.2	Alloy synthesis.....	38
2.2.1	High energy ball milling.....	39
2.2.2	Spark plasma sintering.....	40
2.3	Structural and microstructural characterization.....	42
2.3.1	X-ray diffraction.....	42
2.3.2	Scanning electron microscopy and electron probe micro analyzer.....	44
2.3.3	Transmission electron microscopy.....	45
2.4	Thermal stability.....	46
2.4.1	Differential scanning calorimetry.....	46
2.4.2	Annealing treatment.....	46
2.5	Physical and mechanical properties.....	47
2.5.1	Density calculation.....	47
2.5.2	Microhardness.....	47
2.5.3	Compression test.....	48
2.6	Surface properties.....	48

2.6.1	Wear properties.....	48
2.6.2	Biocompatibility.....	49
2.7	CALPHAD.....	50
2.8	Melting point calculation.....	50
 Chapter 3: Fe₄₀Mn₁₉Ni₁₅Al₁₅Si₁₀C₁ High Entropy Steel.....		52
3.1	Prediction of the melting point.....	52
3.2	Alloying behaviour of the Fe ₄₀ Mn ₁₉ Ni ₁₅ Al ₁₅ Si ₁₀ C ₁ HES.....	53
3.3	Morphology and chemical analysis of the Fe ₄₀ Mn ₁₉ Ni ₁₅ Al ₁₅ Si ₁₀ C ₁ HES powder.....	58
3.4	TEM analysis of milled powder sample.....	60
3.5	Thermal stability of the milled powder sample.....	61
3.6	Structural and microstructural analysis of SPSed sample.....	65
3.7	Physical and mechanical properties of SPSed sample.....	68
3.8	Sliding friction and wear behaviour of the SPSed sample.....	71
3.9	Worn surface morphology of the SPSed sample.....	73
3.10	Biocompatibility of the SPSed sample.....	75
3.11	Discussion.....	76
3.11.1	Alloying behaviour and microstructure.....	76
3.11.2	Thermal stability.....	79
3.11.3	Mechanical properties and strengthening mechanism.....	82
3.11.4	Wear behaviour and biocompatibility.....	86
3.12	Conclusions.....	87

Chapter 4: Fe₄₀Mn₁₄Cr₁₀Ni₁₀Al₁₅Si₁₀C₁ High Entropy Steel.....	89
4.1 Melting point prediction of the Fe ₄₀ Mn ₁₄ Ni ₁₀ Cr ₁₀ Al ₁₅ Si ₁₀ C ₁ HES.....	89
4.2 Alloying behaviour and structural analysis of milled powder sample.....	89
4.2.1 Phase evolution during mechanical alloying of the alloy.....	89
4.2.2 TEM analysis of milled powder sample.....	93
4.2.3 Powder morphology and chemical analysis of milled powder sample.....	95
4.3 Thermal stability and phase evolution of milled powder sample.....	97
4.4 Structural and microstructural analysis of SPSed sample.....	100
4.5 Physical and mechanical properties of the SPSed sample.....	106
4.6 Surface properties of the SPSed sample.....	108
4.6.1 Wear study of the SPSed sample.....	108
4.6.2 In-vitro biocompatibility analysis of SPSed sample.....	111
4.7 Discussion.....	113
4.8 Conclusions.....	120
Chapter 5: Fe₄₀Mn₁₄Ti₁₀Ni₁₀Al₁₅Si₁₀C₁ High Entropy Steel.....	122
5.1 Melting point prediction of the alloy.....	122
5.2 Alloying behaviour of milled powder sample.....	122
5.3 TEM analysis of the powder sample.....	126
5.4 Surface morphology of the mechanically alloyed sample.....	128
5.5 Thermal stability of mechanically alloyed sample.....	129
5.6 Structural analysis of the SPSed sample.....	132
5.7 Microstructural and chemical analysis of the SPSed analysis.....	134
5.8 Physical and mechanical properties of the SPSed sample.....	137

5.9	Wear behaviour of the SPSed sample.....	139
5.10	Biocompatibility of the SPSed sample.....	142
5.11	Discussion.....	144
5.11.1	Phase evolution and formation.....	144
5.11.2	Thermal stability.....	147
5.11.3	Strengthening mechanism.....	149
5.11.4	Wear behaviour and mechanism.....	153
5.12	Conclusions.....	154
 Chapter 6: Fe₄₀Mn₂₀Cr_{20-x}Ni_xTi₁₀Al₁₀ (x =0, 5, and 10 at. %) High Entropy Alloys.....		156
6.1	Melting point prediction of the Fe-based HEAs.....	156
6.2	Alloying behaviour of milled powder samples of Fe-based HEAs.....	158
6.3	Morphology analysis and chemical analysis of Fe-based HEAs.....	162
6.4	Thermal stability of the as-milled powder samples.....	166
6.5	Structural and microstructural analysis of SPSed samples of Fe-based HEAs.....	170
6.6	Physical and mechanical properties of the SPSed sample of Fe-based HEAs.....	174
6.7	Wear behaviour of the SPSed samples of Fe-based HEAs.....	177
6.8	Biocompatibility of the spsed samples of Fe-based HEAs.....	181
6.9	Discussion.....	183
6.9.1	Alloying behaviour and microstructure.....	183
6.9.2	Thermal stability.....	185
6.9.3	Mechanical properties and strengthening mechanism.....	189
6.10	Conclusion.....	193

Chapter 7: Summary and Suggestions for Future Work.....	195
7.1 Summary.....	195
7.2 Suggestions for future work.....	197
References.	199
List of Publications and Patents.....	226
List of Conferences and Workshops.....	227

List of Figures

Figure 1.1:	Development of various materials with the time [19]	2
Figure 1.2:	The lattice distortion in pure metals (BCC), binary alloys, and HEAs are shown schematic [76].....	7
Figure 1.3:	Summary of the four distinct core effects of the HEAs [19].....	8
Figure 1.4:	The effect of configurational entropy, mixing enthalpy and atomic mismatch on the phase formation of the multicomponent HEAs [2].....	11
Figure 1.5:	Relationship between δ and Ω parameters for the multiprincipal alloys. Solid solution (S) indicates that the multiprincipal alloys only form solid solutions. Intermetallics (I) infers that the alloy consisting of majorly intermetallic phase. S+I imply that the alloy composed of solid solution along with intermetallic as precipitates. BMGs demonstrates that the alloy have the amorphous phase (completely) [19].....	12
Figure 1.6:	Summary of the various synthesis routes and its microstructures formed in the high entropy steels and Fe-based HEAs [64, 101, 122, 128, 129].....	16
Figure 1.7:	(a) Total elongation to fracture vs ultimate tensile strength of different types of steels and high entropy steels [60]; (b) Yield strength vs elongation of various conventional alloys and non-equiatomc HEAs [15].....	22
Figure 3.1:	Liquidus temperature ($^{\circ}\text{C}$) values of possible binary compositions in the non-equiatomc FeMnNiAlSiC high entropy steel.....	53
Figure 3.2:	Figure 3.2: (a) XRD patterns of the milled samples at various milling time; (b) Enlarged view along the (110) plane in 2θ range from 49° - 54° ; (c) Blown-up image along the (110) plane; (d) Deconvulated image in between 2θ range from	

	50.5°- 54°. This shows the alloying behaviour of elements with milling time and finally formed the multi-phase structure (BCC, γ -brass type and B2-type) coexisted with trace amount of Si.....	54
Figure 3.3:	(a) XRD pattern of the 35 h milled sample; (b) Reitveld refinement of the corresponding sample. This shows the formation of the multi-phase structure (ferritic as a major phase) after 35 h of milling.....	56
Figure 3.4:	(a-d) SEM micrographs of powder samples milled at different milling time; (d) also marked the full area for EDS analysis; (e) Histograms showing the distribution of the particle size of milled samples at 10 h, 20 h, 30 h and 35 h, respectively. The histogram shows the distribution of the powder particle with the milling time. The average powder particle decreases with the prolongs milling time.....	58
Figure 3.5:	Area elemental mapping of the 35 h green powder sample.....	59
Figure 3.6:	(a) The TEM bright-field image of the 35 h milled sample; (b) its corresponding selected area diffraction ring pattern; (c) Dark field image taken along the (110) plane. Polycrystalline ring pattern corresponds to the BCC phase.....	61
Figure 3.7:	DSC thermogram of milled powder sample of the high entropy steel from 200 °C to 1000 °C.....	62
Figure 3.8:	(a) Ex-situ XRD diffraction pattern of the milled sample at R.T., 400 °C, 500 °C, and 600 °C; (b and c) Deconvoluted peaks for the 500 °C and 600 °C. The formation of Fe ₅ Si ₃ -type intermetallic phase is correlate with exothermic event at 520 °C.....	63

Figure 3.9: (a) XRD pattern of the SPSed pellet; (b) Deconvolution of the SPSed sample ranging from 51°- 54°; (c) Reitveld refinement plot of the SPSed pellet. The ferritic (BCC) type high entropy steel with B2, γ -brass type structure and Fe_5Si_3 type intermetallics can be depicted..... 65

Figure 3.10: (a and b) SEM image of the SPSed sample of the non-equiatomic high entropy steel at different magnifications; (c) Full area EDS analysis of the marked area (in (b)). The different contrast i.e., white (2), light grey (1), dark grey (3) contrast are clearly visible in SEM images..... 66

Figure 3.11: BSE image and EPMA elemental mapping of SPSed sample..... 68

Figure 3.12: (a) Depth of penetration vs Indentation load; (b) Optical micrograph of the indentation spot; (c) Compressive engineering stress and strain curve; (d) Radar diagram. This illustrates the physical and mechanical properties of the SPSed pellet..... 69

Figure 3.13: Figure 3.13: (a, b, c, and d) SEM (SE) micrograph at different magnification of the fractured surface of SPSed sample of the HES1..... 70

Figure 3.14: (a) Change in coefficient of friction (CoF) as a function of time (s) during sliding wear under the various normal load i.e., 5 N, 10 N and 20 N at 10 Hz frequency for SPSed sample; (b) Average coefficient of friction and wear rate against the various normal applied load i.e., 5 N, 10 N and 20 N..... 72

Figure 3.15: SEM (SE mode) micrographs at different magnification of wear fractured SPSed sample of the HES1; (a and b) at 20 N; (c and d) at 10 N; (e and f) at 5 N load condition..... 74

- Figure 3.16:** Concentration-dependent quantitative analysis (MTT assays) of mesenchymal stem cell (MG-63) on control (316L) and SPSed sample of non-equiatomic FeMnNiAlSiC HES after 3, 5 and 7 days. The symbol (◆) represents the statistically significance differences at $p \leq 0.05$ in the mean optical density (O.D.) among the SPSed sample of HES1 with the control sample (316L) treated for 3 days with 5 and 7 days. The symbol (●) represents the statistically differences in the O.D. among all the sample, treated for 5 days with respect to sample treated for 7 days. The symbol (▲) represents the statistically differences in the O.D. among the 316L with high entropy steel sample treated for 7 days..... 75
- Figure 3.17:** Binary enthalpy (kJ/mol) of all the binary alloys in the non-equiatomic FeMnNiAlSiC HES..... 78
- Figure 3.18:** Property diagram represent the phase transformation and phase composition with the function of temperature through CALPHAD modelling (TCFE8) in the non-equiatomic FeMnNiAlSiC high entropy steel. (a) Amount of all the phases versus temperature; (b-f) The elemental composition in all the phases and their stability with respect to temperature..... 82
- Figure 3.19:** (a) The values of the various strengthening mechanism and experimental yield strength (Bar plot); (b) The pie chart for the percentage's contribution of the various strengthening mechanism..... 86
- Figure 4.1:** (a) XRD patterns of the milled samples at various milling time; (b) Enlarged view along the (110) plane in $2\theta = 42^\circ - 46^\circ$. This shows the alloying behaviour

	of alloy with the function of milling time, and it forms the dual-phase structure (BCC and χ -type phase) under 40 h of milling.....	91
Figure 4.2:	(a) XRD pattern of the 40 h milled powder sample; (b) Reitveld refinement of the corresponding sample. This represents the phases formed are dual-phase structure consisting of BCC and χ -phase type structure along with undissolved Si.....	93
Figure 4.3:	(a) TEM bright-field image of the 40 h milled powder sample; (b) its corresponding selected area diffraction ring pattern; (c) dark field image of the 40 h milled powder sample. SAED pattern corresponds to the χ -type phase structure.....	94
Figure 4.4:	(a-d) SEM micrographs of powder samples milled at different milling time i.e., 10 h, 20 h, 30 h and 40 h, respectively. Figure 2(d) also marked the full area for EDS analysis; (e) Full area EDS analysis of 40 h milled powder; (f) Histograms showing the distribution of the particle size of milled samples from top to bottom for 40 h, 30 h, 30 h and 10 h. The histogram shows the distribution of the powder particle with the milling time. The average powder particle decreases with the prolongs milling time.....	95
Figure 4.5:	SEM micrograph of the 40 h milled powder, marked for point EDS analysis and EDS mapping. This shows the area elemental mapping and the elemental overlay. This clearly illustrates that the χ -type phase structure is rich in Fe, Cr and Mn. The unsymmetrical area marked from dotted blue line shows that the Al, Si and C elements is lean in χ -type phase structure.....	97

Figure 4.6: DSC thermogram of the 40 h milled powder of the non-equiatomic FeMnNiCrAlSiC high entropy steel from 200 °C to 1000 °C..... 98

Figure 4.7: (a) Ex-situ XRD diffraction pattern of the milled sample at 25 °C, 400 °C, 600 °C, 700 °C and 900 °C; (b) Enlarge view of diffraction peaks along the (110) plane in $2\theta = 50^\circ$ - 54° ; (c-e) Deconvoluted peaks for the 600 °C, 700 °C and 900 °C, respectively. The formation of Cr₃Si-type intermetallic phase is correlate with exothermic event at 460°C..... 99

Figure 4.8: (a) XRD pattern of SPSed sample; (b) Deconvoluted image along the (111) plane; (c) Reitveld refinement of SPSed sample. The phases formed after the SPSed were FCC as the major phase, B2 as minor phase along with the intermetallics Cr₂₃C₆ and Cr₃Si type..... 102

Figure 4.9: (a) and (b) SEM (BSE) image of the SPSed sample of the high entropy steel at different magnifications; (c) Full area EDS analysis of the marked area (in (b)). The different contrast i.e., light grey (1), dark grey (2) with light and dark grey spherical precipitates are clearly visible in SEM images..... 104

Figure 4.10: Elemental distribution and elemental overlay of the SPSed sample. Mapping shows the uniform distribution of the individual elements..... 105

Figure 4.11: (a) Depth of penetration Vs Indentation load; (b) Optical micrograph of the indentation spot; (c) Compressive stress and strain curve; (d) The radar diagram manifests the physical and mechanical properties of the SPSed sample; (e) The values of the various strengthening mechanism and experimental yield strength (Bar plot); (f) The pie chart for the percentage's contribution of the various strengthening mechanism..... 107

Figure 4.12: SEM micrograph of the fractured sample at different magnifications after the compression test..... 108

Figure 4.13: (a) Coefficient of friction vs time at different load conditions of the SPSed sample; (b) The values of average CoF and specific wear rate at different load condition..... 109

Figure 4.14: Figure 4.14: SEM (SE) micrographs of the worn surface (a) at 5 N; (b) at 10 N; (c) at 20 N. This worn surface at different load condition shows the scratches, ploughing and wear debris features..... 110

Figure 4.15: Concentration-dependent quantitative analysis (MTT assays) of MG-63 on control and SPSed sample after 3, 5, and 7 days. The symbol (♠) represents the statistically differences in the optical density (O.D.) among the SPSed sample with the control sample treated for 3, 5, and 7 days. The symbol (♣) represents the statistically differences in the O.D. among all the sample, treated for 5 days with respect to sample treated for 7 days. The symbol (♥) represents the statistically differences in the O.D. among all the sample treated for 7 days..112

Figure 4.16: Binary enthalpy (kJ/mol) of all the binary pairs in the non-equiatomic FeMnNiCrAlSiC HES..... 114

Figure 4.17: (a) Property diagram of the non-equiatomic FeMnNiCrAlSiC high entropy steel; (b-f) The elemental composition in all the phases and their stability with respect to temperature..... 117

Figure 5.1: (a) XRD pattern of the HES3 powder at various milling time; (b) XRD pattern of the 30 h milled powder. The dual-phase formed during the milling consisting

of BCC ($a = 0.287$ nm) and γ -brass type ($a = 0.890$ nm) structure along with undissolved Si..... 123

Figure 5.2: Reitveld refinement of XRD patterns of milled powder at (a) 20 h; $wR = 2.716$ %, $GoF = 1.07$, and $\chi^2 = 1.15$, (b) 25 h; $wR = 2.637$ %, $GoF = 1.07$, and $\chi^2 = 1.15$, (c) 30 h; $wR = 2.596$ %, $GoF = 1.06$, and $\chi^2 = 1.12$ 125

Figure 5.3: The TEM micrographs of as-milled powder showing (a) bright-field image; (b) corresponding selected area electron diffraction spot pattern. This confirms that the nanocrystalline grains formed with the γ -brass type structure ($Z.A. = [120]$)..... 127

Figure 5.4: The size and shape of the powder particle at (a) 0 h; (b) 10 h; (c) 20 h; (d) 30 h and full area for EDS, and (e) EDS spectrum of the full area. The SEM micrographs exhibit the sizeable river pattern on the surfaces. The distribution of the particle size of powder particles at different milling duration. (f) The histogram exhibit that the particle present in the powders were of different size and their average particle size decreased with the milling time..... 128

Figure 5.5: Area elemental mapping of 30 h of milled powder green compact sample of HES3..... 129

Figure 5.6: DSC thermogram of 30 h milled powder of non-equiatomic FeMnNiTiAlSiC high entropy steel heated up to 1050 °C. The figure shows the phase transformation occurs at T_1 , T_2 , T_3 and T_4 130

Figure 5.7: XRD pattern representing the phases formed during annealing of 30 h milled powder at temperature of 500 °C, 600 °C, 900 °C and 1100 °C. The phases formed were FCC solid solution along with the intermetallics Fe_5Si_3 type and

TiC (in between 600 °C - 900 °C). XRD pattern of the 1100 °C exhibits the change in the amount of phase fraction of the BCC and FCC..... 131

Figure 5.8: (a) XRD pattern of SPSed sample; (b) Enlarge view of the marked area between 48° - 58° ; (c) Reitveld refinement of XRD pattern of SPSed sample of the HES3; $wR = 3.145\%$, $GoF = 1.32$ and $\chi^2 = 1.75$. The phases formed after the sintering (SPS) were FCC as the major phase, BCC as secondary phase along with the intermetallics TiC and Fe_5Si_3 type..... 133

Figure 5.9: (a) and (b) SEM micrograph showing the microstructural features of the SPSed sample of the high entropy steel at different magnifications; (b) Microstructural region SPSed samples investigated for full area EDS analysis; (c) EDS spectrum corresponding to the full area scanning of the microstructure shown in (b). The light grey, dark grey, white and black contrast were marked as 1, 2, 3, and 4, respectively in (b)..... 135

Figure 5.10: Elemental distribution and elemental overlay of SPSed sample of HES3. Mapping shows the uniform distribution of the individual elements..... 136

Figure 5.11: (a) Load-displacement (p-h) curve of SPSed sample of non-equiatomic FeMnNiTiAlSiC high entropy steel; (b) Optical micrograph representing the indent on the surface of SPSed sample; (c) Engineering stress-strain curve of the SPSed sample under compression at room temperature; (d) The radar diagram manifests the physical and mechanical properties of the SPSed sample. The stress and strain curve reveals the ultimate strength and strain of the present alloy were $\sim 2300 \pm 100$ MPa and $\sim 15\%$, respectively..... 138

Figure 5.12: (a, b and c) SEM (SE) micrograph at different magnification of the fractured surface of SPSed sample of HES3. The micrograph shown the shallow dimple and cracks features..... 139

Figure 5.13: (a) Change in coefficient of friction as a function of time (s) for various normal load at 5 N, 10 N and 20 N of the SPSed sample; (b) Average coefficient of friction and specific wear rate against the various normal applied load..... 140

Figure 5.14: SEM (SE mode) micrographs at different magnification of wear fractured SPSed sample of HES3; (a and b) at 5 N; (c and d) at 10 N and (e and f) at 10 N... 141

Figure 5.15: Quantitative assessment of cell density on SPSed and control (316L) specimens on mesenchymal stem cell (MG-63) after 3, 5, and 7 days. The symbol (*) signifies that the statistically difference in the mean optical density (O.D.) among the SPSed sample of HES3 with the control sample (316L) treated for 3 days with 5 and 7 days of control and HES3 samples. The symbol (#) denotes the statistically differences in the O.D. among all the sample, treated for 5 days as with sample treated for 7 days. The symbol (●) symbolises the statistically differences in the O.D. among all the sample treated for 7 days with HES3 sample..... 143

Figure 5.16: Binary enthalpy (kJ/mol) values of all the binary pairs in the non-equiatomic FeMnNiTiAlSiC HES..... 146

Figure 5.17: (a) Property diagram of the non-equiatomic FeMnNiTiAlSiC high entropy steel; (b-f) The elemental composition in all the phases and their stability with respect to temperature..... 149

Figure 5.18: (a) Individual contribution of the various strengthening mechanism for FCC and B2-type phases, and experimental yield strength; (b) Percentage of the individual strengthening mechanism in the HES3..... 153

Figure 6.1: (a) Diffraction patterns of the milled powder of HEA1 samples at 0 h, 10 h, 20 h, 30 h and 40 h; (b) Enlarge view of the diffraction pattern in the range of $2\theta = 42^\circ - 46^\circ$. This shown the alloying behaviour of the elements with milling time, and finally forms the BCC and χ -phase type structure..... 159

Figure 6.2: (a) Diffraction patterns of the milled powder of HEA2 samples at 0 h, 10 h, 20 h, 30 h and 40 h; (b) Enlarge view of the diffraction pattern in the range of $2\theta = 42^\circ - 46^\circ$. This shows the dissolution of the elements with milling durations, and finally forms the dual-phase structure consists of BCC and χ -phase type structure..... 160

Figure 6.3: (a) Diffraction patterns of the milled powder of HEA3 samples at 0 h, 10 h, 20 h, 30 h and 40 h; (b) Enlarge view of the diffraction pattern in the range of $2\theta = 42^\circ - 46^\circ$. This displays the alloying behaviour of the elements with progress of milling time, and at the end of milling its forms the dual-phase structure contains of BCC and χ -phase type structure..... 161

Figure 6.4: (a-d) The microstructural features of the milled powder samples at 10 h, 20 h, 30 h and 40 h of the HEA1; (e) The particle size distribution (histogram plot) of the alloy at 10 h, 20 h, 30 h and 40 h. The size of the particles and average particle size are decreasing with the increase in milling time and it is clearly visible in the histogram plot..... 163

Figure 6.5:	(a-d) The microstructural features of the milled powder samples at 10 h, 20 h, 30 h and 40 h of the HEA2; (e) The particle size distribution (histogram plot) of the alloy at 10 h, 20 h, 30 h and 40 h. The decrease in size of the particles and average particle size with the increase in milling time is clearly visible in the histogram plot.....	164
Figure 6.6:	(a-d) The microstructural features of the milled powder samples at 10 h, 20 h, 30 h and 40 h of the HEA2; (e) The particle size distribution (histogram plot) of the alloy at 10 h, 20 h, 30 h and 40 h. The size of the particles and average particle size are in decreasing trend as the milling time is increases and this trend is clearly visible in the histogram plot.....	164
Figure 6.7:	Elemental mapping of the 40 h green pellet of the HEA1. This illustrates the two-contrast region i.e.; one is Fe rich (BCC phase) and another is Cr and Ti rich (χ -phase type).....	165
Figure 6.8:	Elemental mapping of the 40 h green pellet of the HEA2. This illustrates the two-contrast region i.e.; one is Fe rich (BCC phase) and another is Mn, Cr and Ti rich (χ -phase type).....	165
Figure 6.9:	Elemental mapping of the 40 h green pellet of the HEA3. This illustrates the two-contrast region i.e.; one is Fe rich (BCC phase) and another is Mn, Cr and Ti rich (χ -phase type).....	165
Figure 6.10:	(a, b and c) DSC curve of the 40 h milled sample of the HEA1, HEA2, and HEA3, respectively in between 200 °C to 1000 °C. This curve shows the exothermic events at 500 °C, 540 °C and 510 °C for HEA1, HEA2 and HEA3, respectively.....	167

- Figure 6.11:** (a) Diffraction pattern of the 25 °C, and annealed samples of the HEA1 at 400 °C and 600 °C; (b) Enlarged view in the 2θ range from 42°- 46°. The formation of FCC solid solution was correlated with exothermic events at 500 °C..... 167
- Figure 6.12:** (a) Diffraction pattern of the 25 °C, and annealed samples of the HEA2 at 400 °C and 600 °C; (b) Enlarged view in the 2θ range from 42°- 46°. The formation of FCC solid solution was associated with exothermic events at 540 °C..... 168
- Figure 6.13:** (a) Diffraction pattern of the 25 °C, and annealed samples of the HEA3 at 400 °C and 600 °C; (b) Enlarged view in the 2θ range from 42°- 46°. The formation of FCC solid solution was linked with exothermic events at 510 °C..... 168
- Figure 6.14:** (a, b, and c) Diffraction pattern of the spark plasma sintered sample of HEA1, HEA2, and HEA3, respectively. This shows the formation of BCC and FCC phase in SPSed sample..... 171
- Figure 6.15:** (a, b, and c) Reitveld refinement of the SPSed of HEA1, HEA2, and HEA3, respectively. This also confirms the formation of BCC and FCC along with χ -phase type as precipitates..... 172
- Figure 6.16:** (a, b, and c) The microstructural features (SEM-BSE) of the SPSed sample of HEA1, HEA2, and HEA3, respectively. This shows the two contrast features i.e., light and dark grey, which correspond with the BCC and FCC phase. The light and dark contrast features are marked as 1 and 2 for point EDS analysis..... 173
- Figure 6.17:** (a, b and c) Elemental mapping of the SPSed sample of HEA1, HEA2, and HEA3, respectively..... 174

(a) Depth of penetration Vs Indentation load; (b) compressive engineering stress and strain curve; (a1, a2, and a3) Optical micrograph of the corresponding indentation spot of the HEA1, HEA2, and HEA3, respectively..... 176

Figure 6.18: The microstructural features (SEM-SE) of the fractured surfaces after the compression test of the HEA1, HEA2, and HEA3, respectively..... 177

Figure 6.20: (a, b, and c) Curve between coefficient of friction vs time for the HEA1, HEA2, and HEA3, respectively; (d, e, and f) Coefficient of friction vs time at 20 N, 10 N, and 5 N, respectively..... 178

Figure 6.21: (a, b, and c) SEM (SE) of the worn surface features of the HEA1 at 5 N, 10 N, and 20 N load conditions, respectively; (d, e, and f) HEA2 at 5 N, 10 N, and 20 N, respectively; (g, h, and i) HEA3 at 20 N, 10 N, and 5 N, respectively..... 180

Figure 6.22: Concentration-dependent quantitative analysis (MTT assays) of control (316L) and SPSed samples of HEA1, HEA2, and HEA3 in mesenchymal stem cell (MG-63) after 3, 5, and 7 days. The symbol (*, ♦, ♥) symbolizes the statistically significance differences at $p \leq 0.05$ in the mean optical density (O.D.) among the HEA1, HEA2, and HEA3 with 316L treated for 3, 5, and 7 days, respectively. The statistically significance differences at $p \leq 0.05$ of HEA1 with HEA2 and HEA3 preserved for 3, 5 and 7 days (means (▲, Δ, ●)), respectively..... 182

Figure 6.23: (a) Property diagram of HEA1 (TCFE8); (b-e) Amount of component in the BCC_A2, BCC_A2#2, BCC_A2#3, and liquid, respectively where they are stable in the temperature range..... 187

Figure 6.24: Property diagram of HEA2 (TCFE8). (b-f) Amount of component in the BCC_A2, BCC_A2#3, liquid, BCC_A2#2, and FCC_A1, respectively where they are stable in the temperature range..... 188

Figure 6.25: Property diagram of HEA3 (TCFE8). (b-f) Amount of component in the BCC_A2, BCC_A2#2, BCC_A2#3, FCC_A1, and liquid, respectively where they are stable in the temperature range..... 189

Figure 6.26: (a, b, and c) The values of the various strengthening mechanism and yield strength of the HEA1, HEA2, and HEA3, respectively (Bar plot); (d, e, and f) The pie chart for the percentage's contribution of the various strengthening mechanism of the HEA1, HEA2, and HEA3, respectively..... 192

List of Tables

Table 1.1:	The value of the parameters used to calculate the binary enthalpy ($\Delta H_{\text{mix}}^{\text{ij}}$) [85].....	10
Table 1 2:	Thermal stability of the high entropy steels, Fe-based HEAs and non-equiatomc HEAs.....	19
Table 1.3:	Alloy composition, phases formed, and mechanical properties of various high entropy steels, Fe-based HEAs, and conventional steel prepared using different synthesis routes.....	23
Table 1.4:	Wear properties and cause for improvement/deterioration in wear properties of the various reported high entropy steels, Fe-based HEAs, and non-equiatomc HEAs with different processing routes.....	27
Table 1.5:	The mechanical properties for biomedical applications of HEAs as contrasted to hard tissues.....	30
Table 2.1:	The details of the alloy composition and designations.....	38
Table 2.2:	Atomic percentages to weight percentages for the various alloys.	38
Table 2.3:	Physical and chemical properties of elements used for the synthesis of alloys..	39
Table 2.4:	Parameters for milling of various HEAs powder.....	40
Table 2.5:	Sintering (SPS) parameters of various HEAs.....	41
Table 2.6:	Parameters using during the structural characterization of the powder, annealed and SPSed samples of the alloys.....	43
Table 3.1:	Variation in phase fraction, lattice strain, crystallite size and dislocation density with the function of milling time of powder sample.....	57

Table 3.2:	Elemental composition of 35 h milled powder samples at full area EDS.....	59
Table 3.3:	The phase fraction, lattice parameter and crystallite size of the annealed sample at 400 °C, 500 °C, 600 °C, and SPSed samples of the HES1.....	64
Table 3.4:	Elemental composition of SPSed sample of the HES1 at full area EDS and point WDS.....	68
Table 3.5:	The thermodynamic parameter of the HES1.....	77
Table 4.1:	Variation in phase fraction, lattice strain, crystallite size and dislocation density with the milling time of the powder sample of HES2.....	92
Table 4.2:	The EDS analysis at different location i.e., full area and point EDS for the 40 h milled sample of HES2.....	96
Table 4.3:	The phase fraction, lattice parameter, crystallite size and lattice strain of the annealed sample at 400 °C, 600 °C, 700 °C, 900 °C and SPSed samples of HES2.....	101
Table 4.4:	Elemental composition of SPSed sample of HES2 at full area and point EDS.	105
Table 4.5:	Calculated thermodynamic parameters of the HES2.....	115
Table 5.1:	Variation in phase fraction, crystallite size, microstrain, lattice parameter, and dislocation density during milling.....	126
Table 5.2:	Phase fraction and lattice parameter of the phases formed in the annealed sample at various temperatures and the SPSed sample.....	132
Table 5.3:	Elemental composition of SPSed sample of the non-equiatomic FeMnNiTiAlSiC high entropy steel at point EDS.....	134
Table 5.4:	Thermodynamic parameters values of HES3.....	145

Table 5.5:	Physical meaning and values of different symbols used in the strengthening mechanism calculations.....	151
Table 6.1:	Melting point of the various Fe-based HEAs with different approaches.....	156
Table 6.2:	The value of liquidus temperature of all the binary alloys in the Fe-based HEAs.....	157
Table 6.3:	Lattice parameter, phase fraction, crystallite size, microstrain, and dislocation density of Fe-based HEAs at 30 h, 35 h, and 40 h of milling time.....	162
Table 6.4:	Full area EDS analysis of Fe-based HEAs.....	166
Table 6.5:	The values of the structural and microstructural parameters of the annealed and SPSed samples of the HEA1, HEA2, and HEA3.....	169
Table 6.6:	Full area and point EDS analysis of the HEA1, HEA2, and HEA3 after the SPS.....	173
Table 6.7:	Physical, mechanical and wear properties of the SPSed samples of Fe-based HEAs.....	177
Table 6.8:	Thermodynamic parameter of Fe-based HEAs.....	184
Table 6.9:	Binary enthalpies (kJ/mol) of all possible binary combination in HEA1, HEA2, and HEA3.....	185
Table 7.1:	The comparative assessment in terms of hardness, elastic modulus, yield compressive strength, and wear rate of the various high entropy steels, Fe-based HEAs and 316L.....	197

ABBREVIATIONS

BMGs	Bulk Metallic Glasses
HEAs	High Entropy Alloys
HES	High Entropy Steel
SS	Stainless Steel
MA	Mechanical Alloying
MM	Mechanical Milling
SPS	Spark Plasma Sintering
BCC	Body Centred Cubic
FCC	Face Centred Cubic
HCP	Hexagonal Close Packing
VEC	Valence Electron Concentration
XRD	X-Ray Diffraction
SEM	Scanning Electron Microscopy
EDS/EDX	Energy Dispersive X-ray Spectroscopy
SE	Secondary Electron
BSE	Back Scattered Electron
EPMA	Electron Probe Micro Analyzer

DSC	Differential Scanning Calorimeter
DTA	Differential Thermal Analysis
TEM	Transmission Electron Microscopy
PCA	Process Control Agent
VAM	Vacuum Arc Melting
VIM	Vacuum Induction Melting
PM	Powder Metallurgy
CALPHAD	CALculation of PHAse Diagram
CoF	Coefficient of Friction
ML	Machine Learning
YS	Yield Strength

SYMBOLS

$^{\circ}\text{C}$	Degree Centigrade
a	Lattice Parameter
χ	Chi
ρ	Density
at %	Atomic Percent
wt %	Weight Percent
R	Ideal Gas Constant
Hz	Hertz
χ^2	Reduced least square